A Fast Power Calculation Algorithm for Three-Phase Droop-Controlled-Inverters Using Combined SOGI Filters and Considering Nonlinear Loads

Li, Mingshen; Matas, Jose; Mariachet, Jorge El; Branco, Carlos Gustavo C.; Guerrero, Josep M.

Published in:
Energies

DOI (link to publication from Publisher):
10.3390/en15197360

Publication date:
2022

Document Version
Publisher's PDF, also known as Version of record

energies

MDPI

Article

A Fast Power Calculation Algorithm for Three-Phase Droop-Controlled-Inverters Using Combined SOGI Filters and Considering Nonlinear Loads

Mingshen Li [1], Jose Matas [1,*], Jorge El Mariachet [1], Carlos Gustavo C. Branco [1] and Josep M. Guerrero [2]

[1] Electric Engineering Department, Politechnic University of Catalonia (EEBE-UPC), 08019 Barcelona, Spain
[2] Energy Teknik Department, Aalborg University (ET-AAU), 9220 Aalborg, Denmark
* Correspondence: jose.matas@upc.edu

Abstract: The power calculation is an indispensable element in droop-controlled inverters because the bandwidth of the measured power has a direct impact on the controller performance. This paper proposes a fast and accurate power calculation algorithm based on the combined Second Order Generalized Integrator (SOGI) filters in stationary coordinates for a three-phase system, which takes into consideration the use of nonlinear loads. The power calculation scheme is formed by the two-stage SOGI filters that are employed for obtaining the active and reactive powers required to perform a droop-based inverter operation, respectively. From the two-stage structure, the first SOGI is used as a band-pass filter (BPF) for filtering harmonics and obtaining the fundamental current of the nonlinear load; The second SOGI is used as a low-pass filter (LPF) for extracting the DC-component, which corresponds with the average power. A small-signal model of a two droop-controlled inverters system is built to obtain the dynamical response and stability margin of the system. And compared it with the dynamical behaviour of a standard droop-control method. Next, the proposed power calculation system is designed in order to achieve the same ripple amplitude voltage as that obtained with the standard droop-control method by adjusting the bandwidth gains. Through simulation and hardware in the loop (HIL) validation, the proposed approach presents a faster and more accurate performance when sharing nonlinear loads, and also drives the inverters' output voltage with lower distortion.

Keywords: three-phase paralleled inverters; averaged power calculation; droop-control; SOGI filter; small-signal model; nonlinear loads

Citation: Li, M.; Matas, J.; Mariachet, J.E.; Branco, C.G.C.; Guerrero, J.M. A Fast Power Calculation Algorithm for Three-Phase Droop-Controlled-Inverters Using Combined SOGI Filters and Considering Nonlinear Loads. *Energies* **2022**, *15*, 7360. https://doi.org/10.3390/en15197360

Academic Editor: Nicu Bizon

Received: 13 September 2022
Accepted: 6 October 2022
Published: 7 October 2022

1. Introduction

Microgrid technology and application could be an effective solution for the next-generation power system due to its flexibility and capability to integrate distributed generation sources [1,2]. As interfaces between the distributed resources and a microgrid, the power converters had been investigated in aspects of topology and control [3,4]. colorThe control strategies for power converters such as pulse width modulation (PWM), synchronization technology, and optimal control algorithm. are one of the most important issues of the system. For microgrid typical operating modes, islanded or grid-tied, the converters should have the ability to deliver power to the loads or to the grid. Based on this, several effective control strategies have been proposed, like the droop-control, direct power control, model predictive control, etc. In general, the power calculation is an indispensable part of many controllers, either in rotating or stationary coordinate frames. In addition, due to the low capacity and scattered distribution of DG, the connection of power electronic devices and nonlinear loads not only leads to voltage and current distortions, but also to a poor power harmonic sharing inside a microgrid [5,6].

The droop control is a well-established technique for a parallel inverter system, which is able of sharing the power between the inverters. The control strategy is implemented by

simulating the drooping characteristics of the traditional generators, in which it presents the proportional droop of the active power-frequency and reactive power-voltage curves, respectively. Therefore, the system voltage and frequency are modulated to avoid the circulating current between the paralleled inverters [7–9]. In the standard droop method, a LPF is commonly employed to filter the harmonics and achieve power control accuracy of the active and reactive calculated powers [10–12], because loads in general can induce distortions in the voltage and current. In [13,14], these studies dealt with the virtual impedance and droop improvement by using the first-order LPF. And, the cut-off frequency of this LPF should be designed much smaller than the pass-band of the inverter's voltage control in order to guarantee a proper operation and lower the total harmonic distortion (THD) of the inverter output voltage [15]. For supplying nonlinear loads, ref. [16] proposed a multi-functional controller which employed a second-order LPF to filter the harmonics. In [17], the quantitative analysis of the harmonic powers were studied. In the power calculation stage, a LPF corresponding to the harmonic power calculation was added to the power calculation scheme. However, the lower cut-off frequency of the LPF slows down the system dynamics, and even lead to inverter instability. In [18], the first-order LPF of droop controller was investigated by using the small signal model, and the paper reported that the cut-off frequency has an impact on the dynamic performance, steady-state accuracy and system stability. Ref. [19] presented an nonlinear neural network to improve the power sharing accuracy, particularly for the voltage and frequency regulation in a hierarchical control scheme, in which the LPF is still employed for primary control.

The SOGI filter has been studied to estimate the harmonic components [20,21], in this case, the droop frequency calculation determines and provides the frequency to the SOGI frequency input. Besides, due to the resonance behaviour of the SOGI, the input signal is filtered without delay at the center frequency as a BPF, and the quadrature output is filtered as a LPF. In [22], a virtual impedance loop was designed using a SOGI, which could achieve better output-voltage THD because of the SOGI-BPF capability. In [23], a SOGI filter was used to improve the inherent voltage regulation. However, the power calculation method only filters the double-frequency components and only considers linear loads. In order to improve the transient response and accuracy of the averaged power calculation for nonlinear loads, refs. [24,25] proposed a double structure SOGI filter applied to the current and the power calculation, respectively. However, the method was only applied to single-phase systems.

The presented work seeks to contribute to the improvement of the dynamic behavior and stability for the droop-controlled three-phase voltage source inverter (VSI) when sharing a nonlinear load. The combined SOGI filters are designed to obtain the averaged powers for the droop-control. In this two-stage structure, based on $\alpha\beta$ frame, the fundamental current signals are obtained from the the measured load current through the first-stage SOGI-BPF. Then after the instantaneous power calculation, the second-stage SOGI-LPF is employed to each instantaneous power to acquire averaged power with the less harmonics. The Small-signal model of a two parallel inverters system is formulated to investigate the dynamics performance and stability margin compared with the standard droop-LPF method.

This paper is organized as follows: the control scheme with the combined SOGI filter and comparison with LPF based on droop control are indicated in Section 2. Section 3 presents the small signal analysis and corresponding root locus. The simulation and HIL validation of the proposed method are given in Section 4, including the performance comparison with the LPF-droop method.

2. Combined SOGI Power Calculation Method

The scheme of a VSI controlled by the droop method when sharing a linear or nonlinear load is depicted in Figure 1. In this figure, it can be seen that the control scheme includes the power calculation block, the droop algorithm block, the voltage reference generation,

and PWM block. According to the $\overline{P} - \omega$ and $\overline{Q} - V$ characteristics, the load can be shared among inverters.

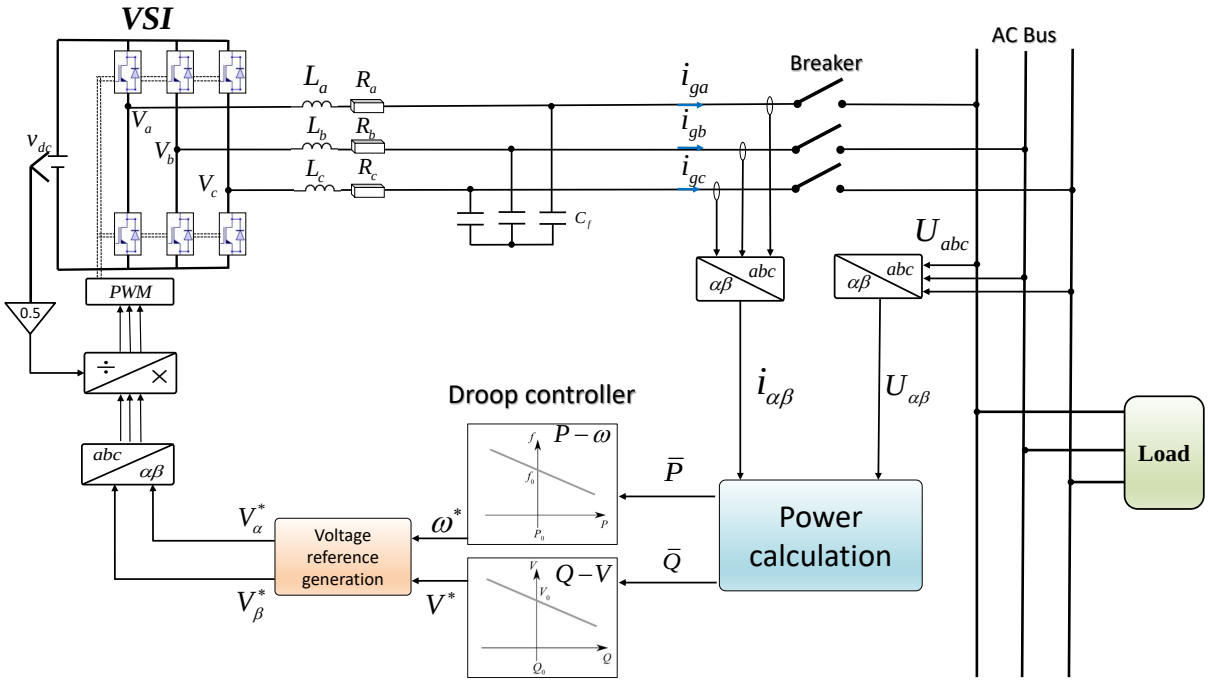

Figure 1. The scheme of the Droop controlled Three-phase inverter in islanded mode.

In order to make the bandwidth of the power controller smaller than the voltage controller and avoid the signal distortion [15], the average power should be calculated by filters. Figure 2 illustrates the conventional average powers calculation and the proposed one for a three-phase system. As shown in Figure 2a, the average powers are obtained by using first-order LPF, whose bandwidth is designed to be much smaller than the bandwidth of the voltage loop. Therefore, motivated by the faster transient response characteristics of the double SOGI, the proposed method is able to be designed as the two stages: the first SOGI is used as a BPF for obtaining fundamental current, and the second SOGI is used as a LPF for extracting DC-component as shown in Figure 2b.

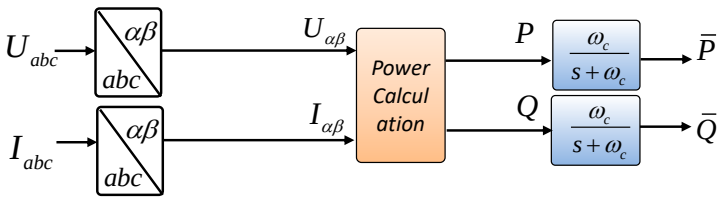

(a) Conventional power calculation method for droop control

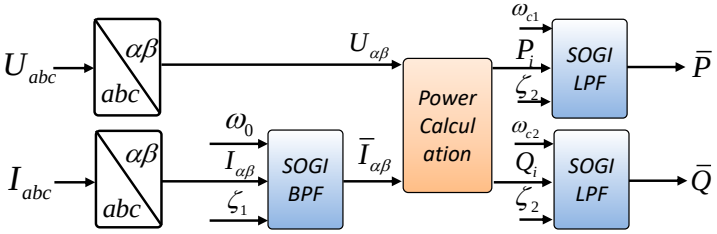

(b) The SOGI power calculation method for droop control

Figure 2. Block diagram of the power calculation schemes: (**a**) conventional LPF filter (**b**) combined SOGI method.

In Figure 3, the nonlinear load is chosen as a three-phase diode-bridge rectifier with a RC load with currents THD that are higher than 25% [26]. In the circuit, the inductor $L = 60\,\mu H$. The capacitance of the RC load is 650 µF, and the resistances of the RC load are $R_{L1} = R_{L2} = 60\,\Omega$.

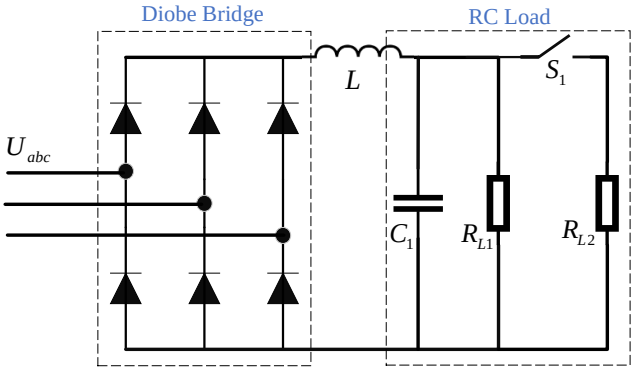

Figure 3. Three-phase Diode-bridge rectifier nonlinear load with a RC load.

According to the Clarke transformation, the inverter voltages and currents can be obtained in the stationary coordinate frame as:

$$v_{\alpha\beta}(t) = T_{\alpha\beta}\begin{bmatrix} v_a(t) \\ v_b(t) \\ v_c(t) \end{bmatrix}, i_{\alpha\beta}(t) = T_{\alpha\beta}\begin{bmatrix} i_a(t) \\ i_b(t) \\ i_c(t) \end{bmatrix}, T_{\alpha\beta} = \frac{2}{3}\begin{bmatrix} 1 & -\frac{1}{2} & -\frac{1}{2} \\ 0 & -\frac{\sqrt{3}}{2} & -\frac{\sqrt{3}}{2} \end{bmatrix} \quad (1)$$

Assuming that the AC bus voltage is balanced and sinusoid. Obviously, the distorted load currents are analysed by using the Fourier series decomposition. Taking the phase A as an example, the load current can be expressed as:

$$i_a = \frac{2\sqrt{3}}{\pi} I_d \sin \omega t + \sum_{n=6k\pm1} (-1)^k \sqrt{2} I_n \sin n\omega t \quad (2)$$

where I_d and n are the rectifier DC-side current and harmonic order, respectively. Therefore, the load current can be decomposed into fundamental and n-order harmonics by using the Clarke transformation.

A SOGI is a linear filter, which provides both the filtered output as well as a quadrature-shifted output as shown in Figure 4. The SOGI in-phase and quadrature-phase outputs behave as BPF and LPF, respectively, with the following transfer functions:

$$G_{BPF}(s) = \frac{2\zeta\omega_c s}{s^2 + 2\zeta\omega_c s + \omega_c^2} \quad (3)$$

$$G_{LPF}(s) = \frac{2\zeta\omega_c^2}{s^2 + 2\zeta\omega_c s + \omega_c^2} \quad (4)$$

where ζ is the damping factor and $\omega_c = 2\pi f_c$ is the tuning center angle frequency. Figure 5 shows the Bode plot of the transfer functions (3) and (4) when the damping factor varies from 0 to 1. It can be observed that the center angle frequency of SOGI is equal to ω_c. In addition, ζ affects the system gain and bandwidth. Considering the phase plot, the phase lag of SOGI-LPF is 90°, and there is almost no phase shift for the lower frequency values for both filters, i.e., <8 Hz.

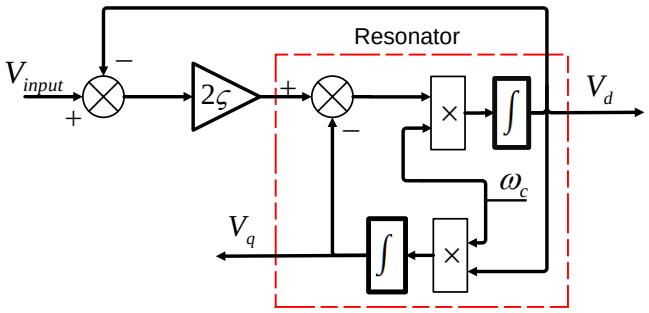

Figure 4. Block diagram of the SOGI filter.

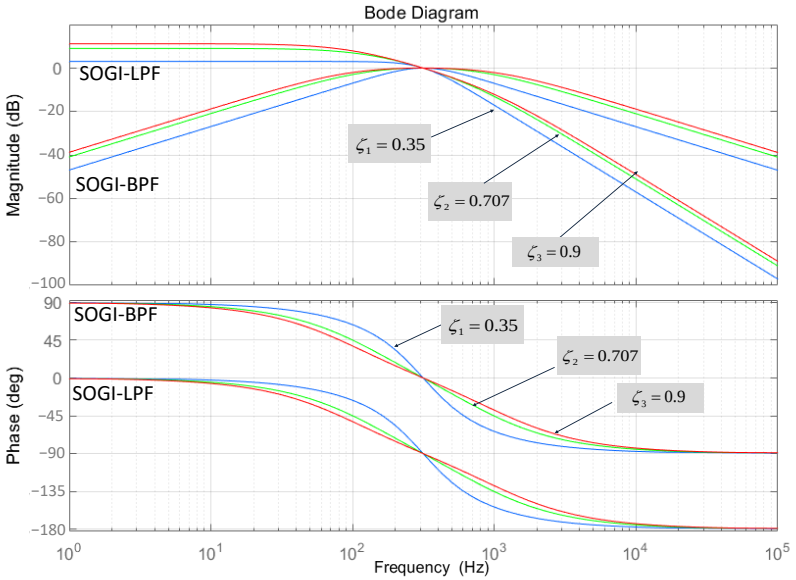

Figure 5. Bode plot of SOGI-LPF transfer function with different damping factors.

In the combined SOGI approach, the first SOGI that acts as a BPF is employed for extracting the fundamental frequency components $\omega_0 = 2\pi f_0$ of the inverter current, so its output signal is synchronized with the input, since there is no phase shift at the center frequency as shown in Figure 5. Considering that there is not a current dc-offset, the filtered current can be expressed as:

$$\begin{aligned} i_{\alpha 0}(t) &= I_{\alpha 0}\sin(\omega t + \varphi_0) \\ i_{\beta 0}(t) &= I_{\beta 0}\cos(\omega t + \varphi_0) \end{aligned} \tag{5}$$

where $I_{\alpha\beta 0}$ are the filtered current amplitudes, which correspond with the amplitude of the fundamental components in stationary coordinate frame, and φ_0 is the phase of the fundamental component.

Therefore, according to (1) and (5), the instantaneous active and reactive power can be formulated as:

$$\begin{aligned} P &= v_\alpha i_{\alpha 0} + v_\beta i_{\beta 0} = 3VI\cos(\omega t) - 3VI\cos(2\omega t - \varphi_0) + 3VI\cos(n\omega t - \varphi_n) \\ Q &= v_\beta i_{\alpha 0} - v_\alpha i_{\beta 0} = 3VI\sin(\omega t) - 3VI\sin(2\omega t - \varphi_0) + 3VI\cos(n\omega t - \varphi_n) \end{aligned} \tag{6}$$

where V and I are the voltage and current amplitudes in $\alpha\beta$ frame, respectively, n is the harmonic components order and φ_n refers to the harmonics phase.

Therefore, instantaneous powers can be expressed as the sum of three components: the averaged powers, the double frequency ripples, and the high order frequency components:

$$\begin{aligned} P(t) &= \overline{P} + \tilde{P} + P_n \\ Q(t) &= \overline{Q} + \tilde{Q} + Q_n \end{aligned} \tag{7}$$

where the superscripts "$-$" and "$\sim$" correspond to the average and the second order frequency oscillating powers, PQ_n are the high order components. In order to remove the double frequency and high order components, an additional SOGI used as a LPF can be employed in next stage where the damping coefficient is ζ_2.

SOGI-BPF will provide the fundamental component of the current with a frequency that corresponds to the operating frequency delivered by the droop-method. Therefore, the signal is going to be in phase with the input, but its envelope is going to track the following first-order transfer function (the cut-off frequency is $\zeta_1\omega_n$). Therefore, the transfer function of the combined SOGI proposal could be expressed as the combination of the previous transfer function cascaded with the transfer function corresponding to the SOGI that acts as a LPF, i.e.,:

$$\begin{aligned} \bar{P}(s) &= \frac{2\zeta_1\zeta_2\omega_n\omega_{c1}^2}{(s+\zeta_1\omega_n)(s^2+2\zeta_2\omega_{c1}s+\omega_{c1}^2)}P(s) \\ \bar{Q}(s) &= \frac{2\zeta_1\zeta_2\omega_n\omega_{c2}^2}{(s+\zeta_1\omega_n)(s^2+2\zeta_2\omega_{c2}s+\omega_{c2}^2)}Q(s) \end{aligned} \tag{8}$$

In order to compare the transient response between double SOGI proposal and the single-LPF corresponding to the standard droop method, the bode plot of two power calculation methods is shown in Figure 6.

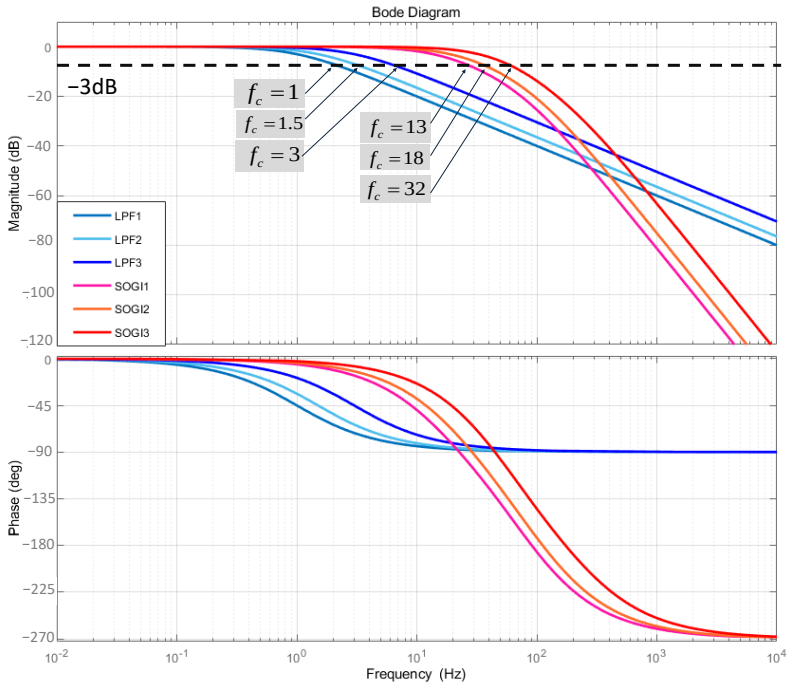

Figure 6. Bode plot of transfer function of the LPF and proposed method with different cut-off requency.

It can be observed that the combined SOGI method behaves a LPF as well, and its cut-off frequency (intersect with -3 dB) is slightly larger than LPF-droop based when their output averaged power are same. Meanwhile, the steady-state phase shit of the combined SOGI filter is $-270°$ at high frequencies due to the fact that (8) is a third-order system. At -3 dB, There are delays for the combined SOGI method, which are similar with the

phase delays of LPF-droop method. Note that the single-LPF is nearly flat when the cut-off frequency varies from 1 Hz to 3 Hz. By contrast, the stop band of the combined SOGI is much narrower than that of the single-LPF even though SOGI's f_c varies from 13 Hz to 32 Hz, which indicates the frequency response of proposed method is faster. It can be concluded that the combined SOGI method is third order LPF-filter, which has the ability to suppress the second and high-frequency components with a fast frequency response.

3. Small Signal Analysis

The objective of this section is to analyse the effects of the conventional and combined SOGI filters' cut-off frequency on the stability and performance of system. The simplified interface circuit for two paralleled VSIs connect to the common AC bus through line impedance is presented in Figure 7. The voltage at the inverter nodes is $E\angle\theta$ referring to an AC bus voltage $U\angle 0$.

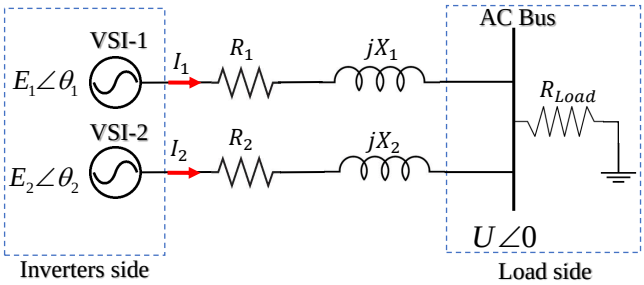

Figure 7. The equivalent circuit of two paralleled VSIs in islanding operation.

Considering an inductive impedance line [15], the active and reactive powers from inverters to the AC bus can be derived as:

$$\begin{aligned} P &= \tfrac{1}{R^2+X^2}(RU^2 - REU\cos\theta + XEU\sin\theta) \\ Q &= \tfrac{1}{R^2+X^2}(XU^2 - XEU\cos\theta - REU\sin\theta) \end{aligned} \tag{9}$$

With regard to the small disturbances, (9) can be linearized at an equilibrium point at steady-state, the disturbance errors of the powers can be expressed as:

$$\begin{aligned} \Delta P &= k_{PE}\Delta E + k_{P\theta}\Delta\theta \\ \Delta Q &= k_{QE}\Delta E + k_{Q\theta}\Delta\theta \end{aligned} \tag{10}$$

where Δ denotes the small deviation of the respective variable from the equilibrium point, and the expansion form of the parameters k are:

$$\begin{aligned} k_{PE} &= \tfrac{1}{R^2+X^2}(2RE - RU\cos\theta + XU\sin\theta) \\ k_{P\theta} &= \tfrac{1}{R^2+X^2}(REU\sin\theta + XEU\cos\theta) \\ k_{QE} &= \tfrac{1}{R^2+X^2}(2XE - XU\cos\theta - RU\sin\theta) \\ k_{Q\theta} &= \tfrac{1}{R^2+X^2}(XEU\sin\theta - REU\cos\theta) \end{aligned} \tag{11}$$

Next, in frequency domain, the small disturbance of frequency and voltage can be given as:

$$\begin{aligned} \Delta\omega(s) &= -m\Delta P = G_f(s)(k_{PE}\Delta E(s) + k_{P\theta}\Delta\theta(s)) \\ \Delta E(s) &= -n\Delta Q = G_f(s)(k_{QE}\Delta E(s) + k_{Q\theta}\Delta\theta(s)) \end{aligned} \tag{12}$$

where m and n are the droop coefficient of the active and reactive powers, respectively, and $G_f(s)$ is the transfer function of the LPF filter used in the power calculation. Substituting $\Delta\omega(s) = s\Delta\theta(s)$ into (10) and (12), the characteristic equation of the system considering the active power loop can be derived as:

$$(nG_f(s)k_{QE}+1)s\Delta\theta(s)+mnG_f{}^2(s)\Delta\theta(s)(k_{P\theta}k_{QE}-k_{PE}k_{Q\theta})+mk_{P\theta}G_f(s)\Delta\theta(s)=0 \quad (13)$$

In order to analyse the effects of the cut-off frequency of the LPF-droop method and of the proposed combined SOGI method, substitute the transfer function of LPF-droop and the proposed method (8) into (13), then the dynamic response of system can be obtained based on the different power calculation methods.

As shown in Figure 8, the root locus for both methods is indicated when the cut-off frequency f_c varies from 0.1 Hz to 1 Hz. For the conventional droop method, the pair of dominant poles move along the negative real axis and towards infinite negative when f_c increases, which implies that the system's dynamic response becomes faster and the system presents overdamped characteristics. In comparison, the dominant poles of the combined SOGI method also are located further from the imaginary axis, and the system indicates an underdamped feature when $f_c = 0.1 \sim 1$ Hz. Thus, the combined SOGI method can be concluded to be faster than the LPF-droop-method considering the same cut-off frequency situation. Moreover, the stability margin of the combined SOGI method is much wider.

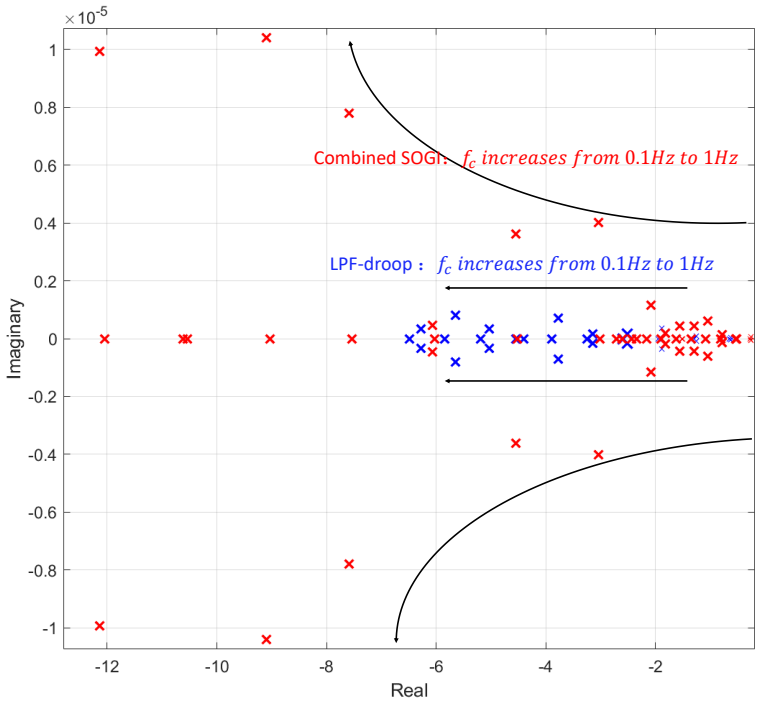

Figure 8. The root locus of the LPF-droop method and the proposed combined SOGI method when f_c varies from 0.1 Hz to 1 Hz.

Figure 9 illustrates the phase response of the two methods. It can be seen that the dynamic response of the proposed method is faster and without oscillation, because the eigenvalues locates near the real axis.

To sum up, from the power calculation perspective, the cut-off frequency will affect the stability and dynamic response of the system, and the larger f_c makes the system faster. To compare with the LPF-droop controller, the proposed method indicates the faster dynamic response and larger stability margin under the same conditions.

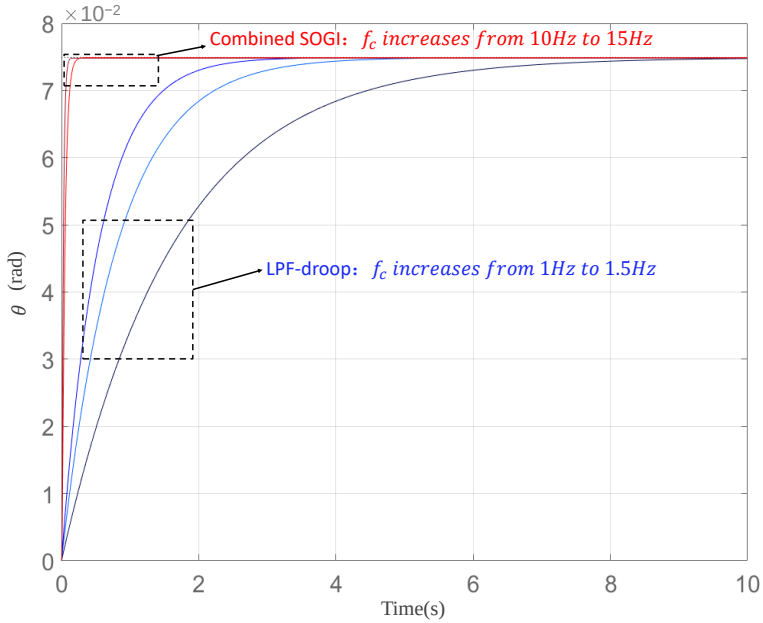

Figure 9. The phase step response of the LPF-droop method and the proposed combined SOGI method when f_c varies from 0.1 Hz to 1 Hz.

4. Simulation and HIL Validation

4.1. Simulation Results

In order to test the performance of proposed combined SOGI method and compare it with the conventional LPF-droop control, the simulation model of two parallel inverters with different types of loads was built under Matlab/PLECS environment. In the simulation model, the electrical system includes the DC source, two three-phase H-bridge inverters, the L filter , transmission line and the shared linear/nonlinear load. The controller block contains two parts: power calculation blocks and droop controller according to Figure 1. Each inverter implements the P-ω and Q-V droop controller with the same slope coefficients, and the parameters of the system are listed in Table 1.

Table 1. System parameters used in simulation.

Paremeters	Value
Nominal output voltage	220 V
Nominal frequency	50 Hz
L-type filter	0.1 Ω + 2 mH
Transmission line	0.01 Ω + 0.32 mH
SOGI-LPF damping coefficient ζ_2	0.707
Active power droop coefficient m	0.001
Reactive power droop coefficient n	0.0001

4.1.1. Case Study I: A Linear Load Step Change

The dynamical performance of two methods under a resistive load step change are illustrated in Figure 10. The cut-off frequency of the LPF-droop controller is designed as 1Hz. For the proposed method, the damping factors of the SOGI-BPF and the SOGI-LPF are all set as 0.707. The center frequency of SOGI-BPF is equal to the instantaneous frequency in P-ω loop, and the cut-off frequency of SOGI-LPF is set to $f_{c1} = 15$ Hz to obtain the same average power as with the LPF-droop method. Figure 10b shows the transient response to an output current step change from 15 A to 30 A supplying a linear load. In this response, from the active power variation of average power, it can be observed that the proposed combined SOGI method is much faster than the LPF-droop method with transient time that

have been measured as 0.05 s and 0.65 s, respectively. Note that there is a small overshoot in the combined SOGI method, which is due to the damping factor.

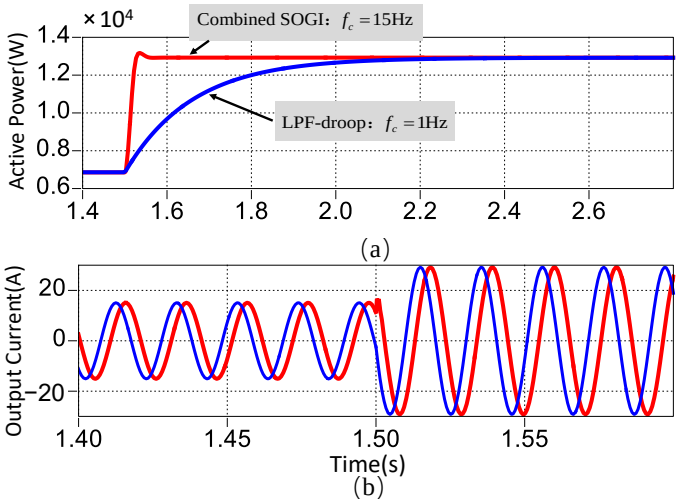

Figure 10. Simulation results for a transient step change in the shared load: (**a**) active powers (**b**) output currents.

4.1.2. Case Study II: f_{c1} Variation Considering a Nonlinear RC Load

On the basis of the root locus analysis shown above, f_c will affect the settling time of the transient response and power ripples. The simulation is further conducted to verify the behaviour under a nonlinear diode bridge rectifier load of THD 28% as shown in Figure 11a. The cut-off frequency of LPF-droop method is designed as 0.3 Hz, and the f_{c1} in the SOGI-LPF of the combined SOGI proposal varies from 7.5 Hz to 30 Hz. When output current perturbation steps from 15 A to 20 A, the dynamic response of the active power is depicted in Figure 12a. The simulation results of the average active power and load voltage are listed in Table 2. when reducing the SOGI-LPF cut-off frequency, the THD of active power with respect to DC component and THD of load voltage are decreasing while the settling time is increasing. In detail, when $f_{c1} = 7.5$ Hz, the THD of $\bar{P}$ and V_L fall down to 0.587% and 7.74%, respectively, while keeping an longer settling-time 0.162 s. Meanwhile, when f_{c1} increases, the power ripple increases, and the power THD reaches to 1.331% with a shorter settling time 0.078 s. It indicates that simulation results are in consistency with the theoretical analysis.

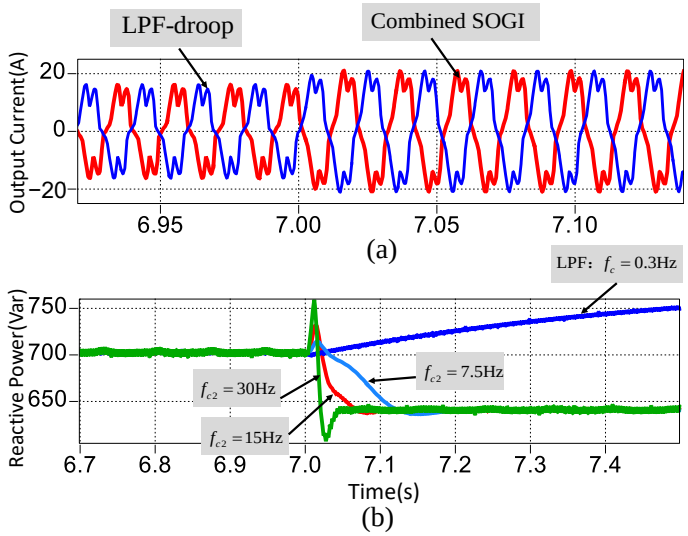

Figure 11. Simulation results for a nonlinear RC load under f_{c2} variation: (**a**) output current. (**b**) reactive power.

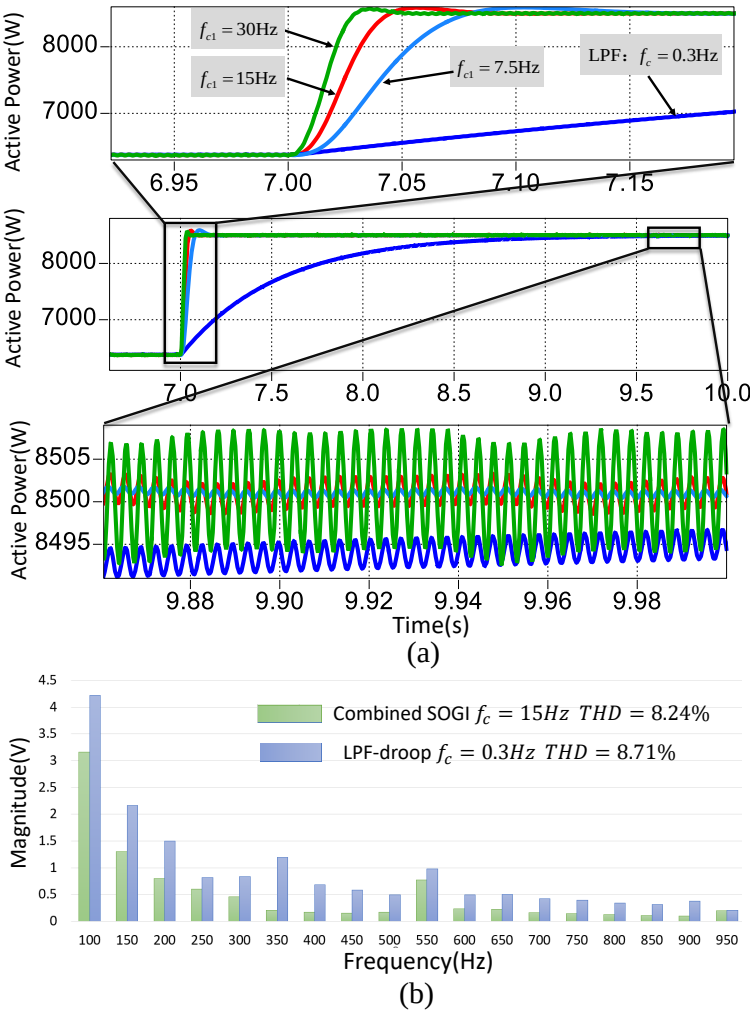

Figure 12. (**a**) The active power for a nonlinear RC load under f_{c1} variation. (**b**) THD of load voltage.

Table 2. Simulation results for THD of load voltage, THD and settling time of active power.

	THD of $\bar{P}$	THD of V_L	Settling Time/% Reduction
LPF-droop $f_{c1} = 0.3$ Hz	0.932%	8.71%	2.15 s/-
Combined SOGI $f_{c1} = 30$ Hz	1.331%	9.05%	0.078 s/96.37%
Combined SOGI $f_{c1} = 15$ Hz	0.941%	8.24%	0.096 s/95.5%
Combined SOGI $f_{c1} = 7.5$ Hz	0.587%	7.74%	0.162 s/92.5%

In order to compare the transient response fairly, the power ripple of both methods should be regulated equally. The peak-peak value for SOGI and LPF is approximately equal to about 3.5 W, as shown in Figure 12a scaled active power, where SOGI's f_{c1} is 15 Hz and LPF's is 0.3 Hz. In this case, the THD of both methods is approximately equal to 0.932%, but the settling time of the combined SOGI has a remarkable reduction with 95.5%. Regarding the THD of load voltage, the combined SOGI's 8.25% is slightly smaller than the LPF's 8.71% as shown in Figure 12b. It can be concluded that the dynamic response of the combined SOGI is much faster than LPF-droop, and a lower THD of load voltage is achieved. Next, the reactive power dynamic responses of two methods are different because there is no inductive loads in Figure 11b.

4.1.3. Case Study III: f_c2 Variation Considering a Nonlinear RL Load

Considering the inductive loads, Figure 13a depicts the dynamic response of the reactive power with a variation of less than 600 Var. The power factor has changed from 1 to 0.99746 since 2.5 s. Table 3 presents ThD of load voltage, THD and the settling time of the reactive power, where the LPF-droop's settling-time is the worst with a value of 2.84 s. On the other hand, the best time is obtained by the combined SOGI algorithm with a higher reactive power THD of 0.894%. Considering the approximate THD of $\bar{Q}$, the settling time is reduced to 97.3% if the cut-off frequency f_{c2} is 15 Hz for the combined SOGI, in which the peak-peak $\bar{Q}$ ripple value is approximately equal to 3 Var, and the load voltage of combined SOGI has less distortion with 6.61% compared with the LPF-droop's 6.78% as shown in Figure 13b.

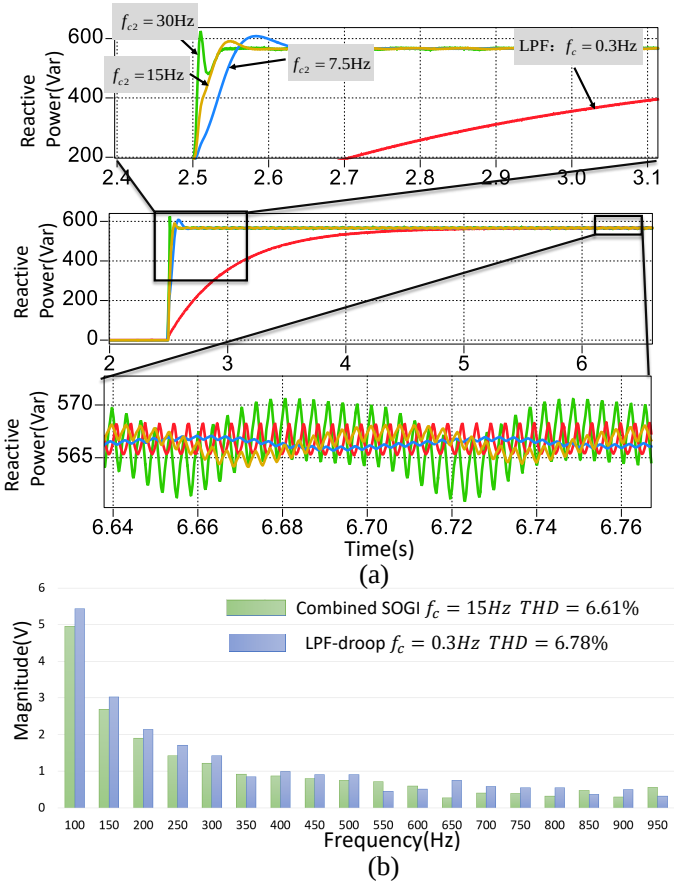

Figure 13. (**a**) The reactive power for a nonlinear RL load under f_c variation. (**b**) THD of load voltage.

Table 3. Simulation results for THD of load voltage, THD and settling time of reactive power.

	THD of $\bar{Q}$	**THD of V_L**	**Settling Time/% Reduction**
LPF-droop $f_{c2} = 0.3$ Hz	0.621%	6.78%	2.84 s/-
Combined SOGI $f_{c2} = 30$ Hz	0.894%	6.98%	0.064 s/97.7%
Combined SOGI $f_{c2} = 15$ Hz	0.614%	6.61%	0.076 s/97.3%
Combined SOGI $f_{c2} = 7.5$ Hz	0.443%	6.36%	0.124 s/95.6%

In this conditions, the settling time of the combined SOGI is about 0.08 s compared to the LPF-droop's that is 2.28 s, which indicates that the combined SOGI method is much faster than the LPF-droop method. In addition, when f_{c2} is decreased the transient is slower and the steady-state ripple is smoother. Due to the lower f_{c2}, it will filter more harmonics components of the power ripple, which leads to a slower dynamics response.

4.1.4. Case Study IV: ζ_1 Variation Considering a Nonlinear RC Load

In this case, the damping ratio of SOGI-BPF is changed from 0.56 to 0.9 considering a nonlinear RC loads. In order to achieve the same power ripple, f_c is regulated as 15 Hz and 0.3 Hz for the combined SOGI and LPF-droop methods, respectively. In Figure 14, the transient response of the active power slows down when ζ_1 is increased, but it performs faster dynamics than LPF-droop clearly. Furthermore, the RMS value of the active power has been reduced when $\zeta_1 = 0.56$, because the amplitude of current decreases through the smaller damping ratio of SOGI filter.

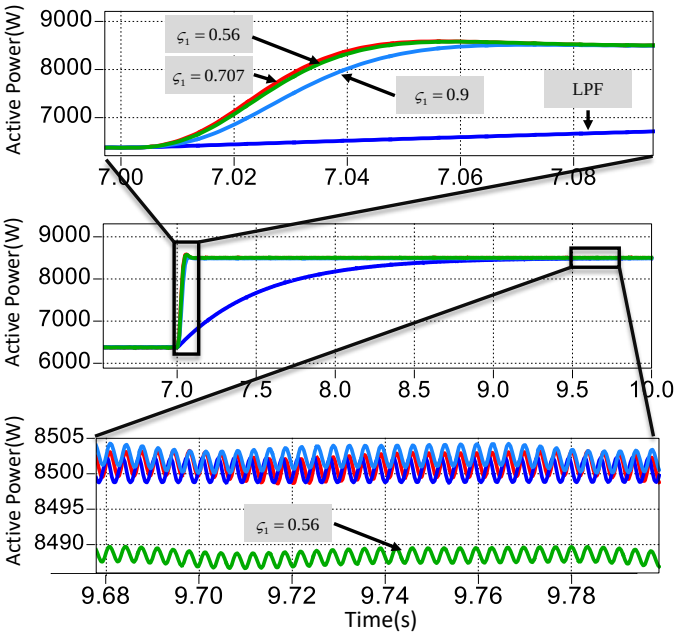

Figure 14. The active power under ζ_1 variation.

Figure 15a presents the nonlinear load current of the two methods when the load step at 7 s. The circulating current between the inverters is almost zero for both methods, as shown in Figure 15b, which means the power is shared between the two inverters. For the sake of standard design, ζ_1 is usually designed to be 0.707 as a well-known optimal trade-off. In order to achieve the accurate power, the damping ratio can be regulated based on the standard value.

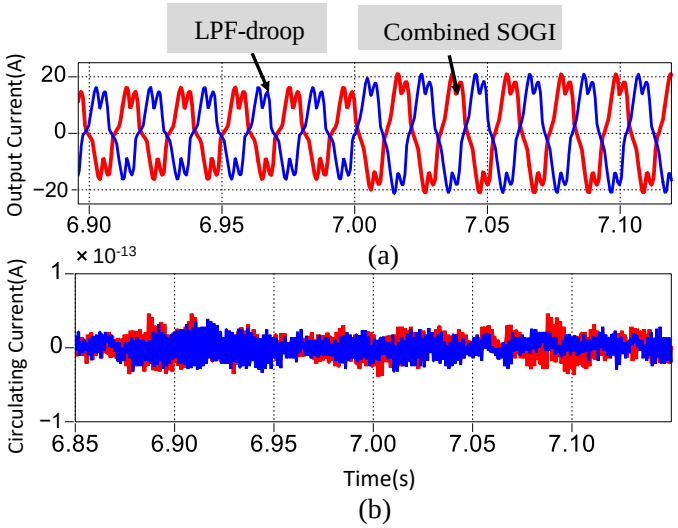

Figure 15. (**a**) The load current and (**b**) circulating current under ζ_1 variation.

4.2. HIL Assessment Results

The performance of the combined SOGI method is also validated by Typhoon HIL control platform. The controller parameters are same as the simulation. The switching frequency of the VSI is chosen as 10 kHz. For the digital implementation of the combined SOGI based on (3) and (4), the third-order integrator is used to obtain a lower residual ripple of the amplitude and frequency signals [27]:

$$G_{Int}(z) = \frac{T_s(23z^{-1} - 16z^{-2} + 5z^{-3})}{12(1 - z^{-1})} \tag{14}$$

Figure 16 shows the transient response for both methods during the nonlinear RC load step changing. In order to achieve the same active power ripple as 3.5 W (as shown in Figure 16a), the cut-off frequency for the combined SOGI and LPF-droop is set to 15 Hz and 0.3 Hz, respectively. It can be seen that a significantly faster transient response by the combined SOGI is achieved with 0.15 s compared to the LPF-droop's 3.6 s, which has 95.8% settling time reduction. Figure 16b,c illustrate the transient of output current and load voltage during this sudden load change. The THD of load voltage for the combined SOGI and LPF is measured as 8.64% and 8.89%, respectively. Thus, the HIL results are similar to the simulation results.

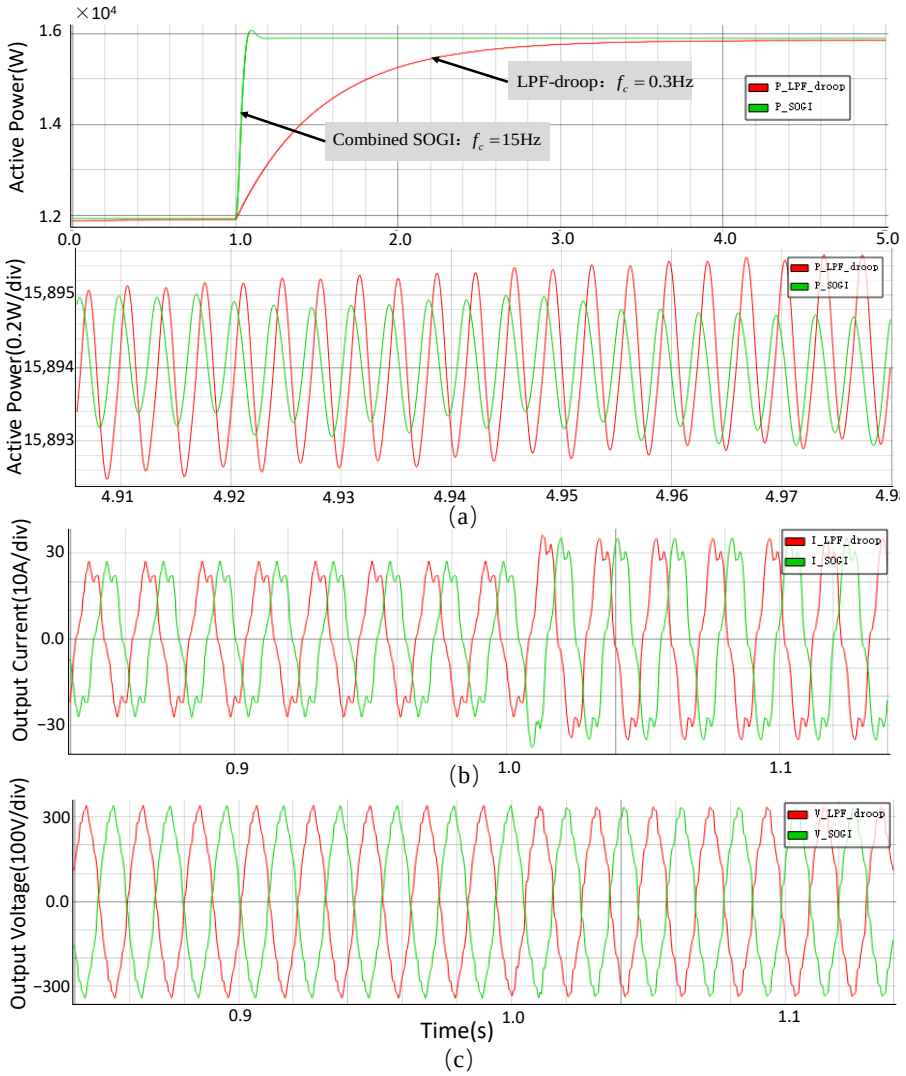

Figure 16. HIL emulation for a nonlinear RC load step change in the shared load. (**a**) active power and its scaled waveform in steady-state. (**b**) output current. (**c**) load voltage.

Thus, the simulation and HIL results demonstrate that the proposed technique performs a faster dynamics response compared with the LPF-droop when the inverters are sharing the linear and nonlinear loads. With the same power ripple, a measured time reduction of the combined SOGI arrives around 95% for $\bar{P}$ and $\bar{Q}$, which improves the dynamic performance of the system while the inverters are working in parallel or in islanded microgrids applications.

5. Conclusions

In this work, a fast and accurate power calculation method based on a combined SOGI filter approach for the parallel three-phase inverters in the presence of nonlinear loads has been proposed. In comparison with the conventional droop controller, the proposed method is demonstrated to achieve a faster performance, which is motivated by the synchronization and signal extraction accuracy of SOGI filters. Based on the small signal model of two parallel inverters, the root locus and phase step response presented faster dynamic response compared with the LPF-based droop method. Then, the cut-off frequency is further designed based on the same ripple as LPF method to proof the performance of the proposed method. Next, the damping ratios are discussed considering the transient response. A series of simulations were carried out to validate the combined SOGI method and compare it with LPF under supplying the linear and nonlinear loads. In simulation and HIL validation, the transient time of the combined SOGI method has near 95% reduction with the same power ripple. The obtained results verified the effectiveness and the faster dynamics in the presence of both linear and nonlinear loads. As part of future work, the virtual impedance loops should be considered with the combined SOGI. Thus, the reactive power sharing control would be designed based on the proposed filter.

Author Contributions: Investigation, equations derivation and writing—original draft preparation, M.L. and J.M.; methodology and simulation results, M.L. and J.E.M.; data curation J.E.M. and C.G.C.B.; proof reading and review J.M. and J.M.G. organization and format editing, M.L. and J.M.G. All authors have read and agreed to the published version of the manuscript.

Funding: This research received no external funding.

Data Availability Statement: Not applicable.

Conflicts of Interest: The authors declare no conflict of interest.

References

1. Shayeghi, H.; Shahryari, E.; Moradzadeh, M.; Siano, P. A survey on microgrid energy management considering flexible energy sources. *Energies* **2019**, *12*, 2156. [CrossRef]
2. Hossain, M.A.; Pota, H.R.; Issa, W.; Hossain, M.J. Overview of AC microgrid controls with inverter-interfaced generations. *Energies* **2017**, *10*, 1300. [CrossRef]
3. Jiayi, H.; Chuanwen, J.; Rong, X. A review on distributed energy resources and MicroGrid. *Renew. Sustain. Energy Rev.* **2008**, *12*, 2472–2483. [CrossRef]
4. Olivares, D.E.; Mehrizi-Sani, A.; Etemadi, A.H.; Cañizares, C.A.; Iravani, R.; Kazerani, M.; Hajimiragha, A.H.; Gomis-Bellmunt, O.; Saeedifard, M.; Palma-Behnke, R.; et al. Trends in microgrid control. *IEEE Trans. Smart Grid* **2014**, *5*, 1905–1919. [CrossRef]
5. Borup, U.; Blaabjerg, F.; Enjeti, P.N. Sharing of nonlinear load in parallel-connected three-phase converters. *IEEE Trans. Ind. Appl.* **2001**, *37*, 1817–1823. [CrossRef]
6. De, D.; Ramanarayanan, V. Decentralized parallel operation of inverters sharing unbalanced and nonlinear loads. *IEEE Trans. Power Electron.* **2010**, *25*, 3015–3025. [CrossRef]
7. De Brabandere, K.; Bolsens, B.; Van den Keybus, J.; Woyte, A.; Driesen, J.; Belmans, R. A voltage and frequency droop control method for parallel inverters. *IEEE Trans. Power Electron.* **2007**, *22*, 1107–1115. [CrossRef]
8. Nasirian, V.; Davoudi, A.; Lewis, F.L.; Guerrero, J.M. Distributed adaptive droop control for DC distribution systems. *IEEE Trans. Energy Convers.* **2014**, *29*, 944–956. [CrossRef]
9. Vasquez, J.C.; Guerrero, J.M.; Luna, A.; Rodríguez, P.; Teodorescu, R. Adaptive droop control applied to voltage-source inverters operating in grid-connected and islanded modes. *IEEE Trans. Ind. Electron.* **2009**, *56*, 4088–4096. [CrossRef]
10. Deng, W.; Dai, N.; Lao, K.W.; Guerrero, J.M. A virtual-impedance droop control for accurate active power control and reactive power sharing using capacitive-coupling inverters. *IEEE Trans. Ind. Appl.* **2020**, *56*, 6722–6733. [CrossRef]

11. Li, Z.; Chan, K.W.; Hu, J.; Guerrero, J.M. Adaptive droop control using adaptive virtual impedance for microgrids with variable PV outputs and load demands. *IEEE Trans. Ind. Electron.* **2020**, *68*, 9630–9640. [CrossRef]
12. Zhang, W.; Zheng, Z.; Liu, H. A novel droop control method to achieve maximum power output of photovoltaic for parallel inverter system. *CSEE J. Power Energy Syst.* 2021, *early access*.
13. Lu, F.; Liu, H. An Accurate Power Flow Method for Microgrids with Conventional Droop Control. *Energies* **2022**, *15*, 5841. [CrossRef]
14. Buraimoh, E.; Aluko, A.O.; Oni, O.E.; Davidson, I.E. Decentralized Virtual Impedance-Conventional Droop Control for Power Sharing for Inverter-Based Distributed Energy Resources of a Microgrid. *Energies* **2022**, *15*, 4439. [CrossRef]
15. Coelho, E.A.A.; Cortizo, P.C.; Garcia, P.F.D. Small-signal stability for parallel-connected inverters in stand-alone AC supply systems. *IEEE Trans. Ind. Appl.* **2002**, *38*, 533–542. [CrossRef]
16. Vasquez, J.C.; Mastromauro, R.A.; Guerrero, J.M.; Liserre, M. Voltage support provided by a droop-controlled multifunctional inverter. *IEEE Trans. Ind. Electron.* **2009**, *56*, 4510–4519. [CrossRef]
17. Wang, W.; Zeng, X.; Tang, X.; Tang, C. Analysis of microgrid inverter droop controller with virtual output impedance under non-linear load condition. *IET Power Electron.* **2014**, *7*, 1547–1556. [CrossRef]
18. An, R.; Liu, J.; Wu, T.; Wang, S.; Liu, B. Analysis and design of cutoff frequency for power calculation low-pass filters in droop control. In Proceedings of the 2017 IEEE 3rd International Future Energy Electronics Conference and ECCE Asia (IFEEC 2017-ECCE Asia), Kaohsiung, Taiwan, 3–7 June 2017; pp. 1596–1600.
19. Baghaee, H.R.; Mirsalim, M.; Gharehpetian, G.B. Power calculation using RBF neural networks to improve power sharing of hierarchical control scheme in multi-DER microgrids. *IEEE J. Emerg. Sel. Top. Power Electron.* **2016**, *4*, 1217–1225. [CrossRef]
20. Matas, J.; Martin, H.; de la Hoz, J.; Abusorrah, A.; Al-Turki, Y.A.; Al-Hindawi, M. A family of gradient descent grid frequency estimators for the SOGI filter. *IEEE Trans. Power Electron.* **2017**, *33*, 5796–5810. [CrossRef]
21. Matas, J.; Martín, H.; de la Hoz, J.; Abusorrah, A.; Al-Turki, Y.; Alshaeikh, H. A new THD measurement method with small computational burden using a SOGI-FLL grid monitoring system. *IEEE Trans. Power Electron.* **2019**, *35*, 5797–5811. [CrossRef]
22. Matas, J., J.M.; Castilla, M.; De Vicuña, L.G.; Miret, J.; Vasquez, J.C. Virtual impedance loop for droop-controlled single-phase parallel inverters using a second-order general-integrator scheme. *IEEE Trans. Power Electron.* **2010**, *25*, 2993–3002.
23. Tolani, S.; Sensarma, P. An improved droop controller for parallel operation of single-phase inverters using RC output impedance. In Proceedings of the 2012 IEEE International Conference on Power Electronics, Drives and Energy Systems (PEDES), Bengaluru, India, 16–19 December 2012; pp. 1–6.
24. El Mariachet, J.; Guan, Y.; Matas, J.; Martín, H.; Li, M.; Guerrero, J.M. HIL-assessed fast and accurate single-phase power calculation algorithm for voltage source inverters supplying to high total demand distortion nonlinear loads. *Electronics* **2020**, *9*, 1643. [CrossRef]
25. El Mariachet, J.; Matas, J.; Martín, H.; Li, M.; Guan, Y.; Guerrero, J.M. A power calculation algorithm for single-phase droop-operated-inverters considering linear and nonlinear loads HIL-assessed. *Electronics* **2019**, *8*, 1366. [CrossRef]
26. Wallace, I. Key Changes and Differences between the New IEEE 519-2014 Standard and IEEE 519-1992. *Alcatel Telecommun. Rev.* **2014**, *11*.
27. Rodriguez, F.; Bueno, E.; Aredes, M.; Rolim, L.; Neves, F.A.; Cavalcanti, M.C. Discrete-time implementation of second order generalized integrators for grid converters. In Proceedings of the 2008 34th Annual Conference of IEEE Industrial Electronics, Orlando, FL, USA, 10–13 November 2008; pp. 176–181.